Proceedings of the Project Review, Geo-Mathematical Imaging Group (Purdue University, West Lafayette IN), Vol. 1 (2012) pp. 295-304.

FROM LABORATORY TO FIELD–CRITICAL SCALING OF SINGLE FRACTURES

CHRISTOPHER PETROVITCH*, LAURA J. PYRAK-NOLTE†, AND DAVID D. NOLTE‡

Abstract. Experimental work suggests that the flow-stiffness relationship in single fractures relies on the geometry of the fracture, i.e. the size and spatial distributions of the void and contact areas. It is useful to understand the scaling of these distributions in relation to the hydromechanical properties of fractures. This would allow studies conducted on smaller laboratory samples to be understood on the field scale. In this study, the difficulties associated with interpreting measurements taken in the laboratory are uncovered and it is shown that the scaling is in fact fundamentally different. Finite-size scaling methods were used to extract critical thresholds for fractures under load and flow exponents were extracted. This allows the full hydromechanical coupling to be understood in both Effective Medium and Critical regimes.

1. Introduction. In today's world, society rely upon the earth's subsurface in many ways. These include the extraction of drinkable water; production of oil and gas; nuclear waste disposal; the storage of anthropogenic byproducts (e.g. CO_2) in subsurface reservoirs; the construction of subsurface structures, such as tunnels and underground buildings; and the foundations of dams and bridges. To successfully plan for any of these projects, an understanding of the geologic structures in the subsurface is required. This knowledge is very difficult to obtain because the earth's subsurface is composed of a hierarchy of processes which occur at scales that span many orders of magnitude. In this paper, the authors use the term fracture to refer to mechanical discontinuities that range in scale from lattice dislocations (10^{-9} m) to micro-cracks (10^{-6} m) to fractures (1 m) to the scale of plate boundaries (10^4 m).

To study processes with this range of scales, many scientists turn to the framework provided by Percolation Theory and more specifically finite-size scaling methods. Percolation Theory has been successfully used to predict many other physical processes that occur at different scales, such as, phase transitions, the spreading of forest fires, and the electrical conductance through random mediums [15]. The first step is to understand when a physical process is in an *Effective Medium* or *Critical Scaling* regime. Effective Medium scaling occurs when the scale of the system is not a dominating factor in the physical process of interest. For example, when considering fluid flow through two parallel plates, the flow is dominated by the "cubic law." Critical scaling occurs when the scale of the system becomes the dominating factor. So, if one randomly placed pillars between the parallel plates, eventually the pillars would be so densely-packed that the flow paths would be cut off. At and around this point, called a critical *threshold*, the "cubic law" no longer dominates the flow rate, and a clear scale dependence emerges. Then the framework of finite-size scaling can be used to remove this dependence so that the flow is understood at all scales within the critical regime.

In this study, the authors wish to describe the scaling relationship between the mechanical property–fracture specific stiffness–and the hydraulic property–permeability–in single fractures. This study was conducted computationally, using a stratified percolation method to generate the fracture geometries [11, 9, 10], a deformation model developed by Hopkins [6], and a fluid flow solver which converted the fracture geometry to a network of elliptical pipes [17]. To begin understanding the hydromechanical scaling the authors split the problem into three subproblems.

Firstly, the generation and flow codes were tested using geometries with constant aperture. Secondly, the authors begin to distinguish the difference between taking stiffness measurements in the laboratory and the field. Measurements taken in the lab usually involve small samples placed under a constant displacement load. The consequence of this is having free boundary conditions along the edge of the fracture plane, which can have large effects on the scaling of the permeability.

*Department of Physics, Purdue University, West Lafayette, IN

†Department of Physics, Department of Earth and Atmospheric Science, and School of Civil Engineering, Purdue University, West Lafayette, IN

‡Department of Physics, Purdue University, West Lafayette, IN

TABLE 2.1
Parameters used to generate uncorrelated fractures in this scaling study.

L (pxl)	L (m)	NPTS
32	0.0625	146
64	0.125	590
128	0.23	2357
256	0.5	9445
512	1.0	37726

On the other hand, field measurements are usually extracted from seismic reflection data. This will measure the stiffness in a localized region of a larger fracture. This difference in boundary conditions had a large effect on the critical scaling regime and a critical threshold was only extracted for the field-type fractures. Lastly, the hydromechanical scaling relationship is considered for field-type fractures. The scale dependence was removed from the permeability with a standard finite-size scaling approach and then used to collapse the full hydromechanical relationship.

2. Fracture Model. In this study, the simulated fracture void geometries were generated using a stratified percolation method [11, 9, 10]. While many methods are based on bringing two generated rough surfaces together, (Pietgen & Saupe, [12]; Brown, [1]; Glover et al., [4]; Borodich & Onishchenko, [1]; Walsh et al., [18]) , the stratified percolation method enables the user to control the void spaces directly, rather than indirectly. This method constructs a two-dimensional hierarchical aperture distribution with a tunable spatial correlation. The construction begins with a two-dimensional array set to zero. This initial array is termed the first tier. Within that tier, NPTS (number of points per tier) points are selected and used to define the center of the next tier. This next tier is scaled down by a scale factor, b. This process is repeated until the desired number of tiers have been generated. Finally, within the final tiers, NPTS points of a given size are randomly picked and the initial two-dimensional array is incremented by one unit. Overlapping tiers result in spatially-correlated aperture distributions. In this work, the authors refer to *uncorrelated* generations as fractures with only one tier, while *correlated* generations have the full hierarchical structure. Examples of both specially uncorrelated and correlated fractures are shown in Figure 1. In this study, only uncorrelated fractures were studied. Fractures were generated using the parameters listed in Table 2.1. The five scales ranged from 0.0625m to 1.0m providing approximately an order of magnitude range in scale. The parameters were chosen such that the initial contact area was approximately 5% of the fracture plane.

3. Deformation Model. Understanding how a fracture deforms when subject to a load is necessary when investigating the relationship between the mechanical and hydraulic properties of fractures. In this study, fractures were deformed numerically under a normal load using a method similar to that developed by Hopkins [6]. Hopkins' model assumes a joint can be approximated by two parallel half-spaces separated by an asperity distribution. This model is similar to Greenwood & Williamson's model [5] where the joint was modeled as an asperity distribution in contact with a flat and rigid surface, and it's later improvement by Brown and Scholtz [2] where the joint was modeled as two rough surfaces in contact. Unlike these models, Hopkins' included the interaction between contact points by allowing each of the half-spaces to deform about the asperities as well as the asperity deformation and it did not allow interpretation of the two rough surfaces like Brown and Scholtz [2]. Each asperity is modeled as a cylinder arranged on a regular lattice. The height of each cylinder is determined by the fracture generation model and is given a radius such that all cylinders initially are in contact with neighboring cylinders.

A linear system of equations can be written for this system by noting that for each asperity, the sum of the initial distance between the half-spaces, D, and the total deformation , W_i, must equal

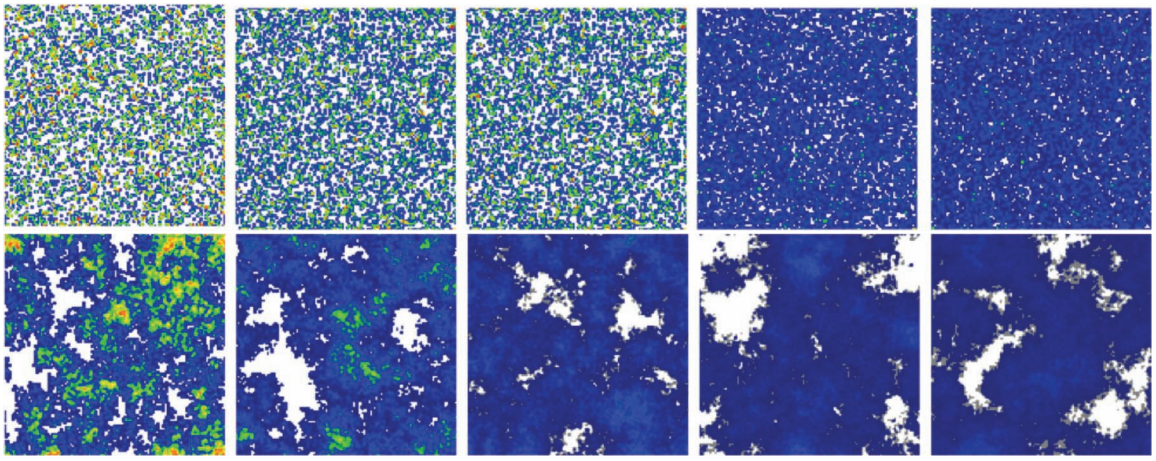

FIG. 1. *Example fractures generated on a 256 by 256 grid with a point size of 4 by 4. (Top row) Uncorrelated synthetic fractures generated with NPTS = 3800, 5000, 6600, 9700, 12400. (Bottom row) Correlated synthetic fractures generated with NPTS = 12, 14,16, 18, 20 and the scale factor is set such that the final tier is the size of a point. The white areas are contact areas, while the color range blue to red are increasing apertures.*

the length of the asperity, or

$$D + W_i = h_i + \Delta h_i \qquad \text{for } i \in C, \tag{3.1}$$

where C is the set of all apertures in contact, and the change in height, Δh_i is the unknown variable. The total displacement is the superposition of the self-interaction, displacement of asperity i due to the deformation of the half-space by asperity i, and the asperity-asperity interaction, displacement of asperity i due to the deformation of the half-space by asperity j. The displacement of the half-space, w_0, is found by integrating the Boussinesq's solution for a loaded circle [16]. The solution is divided into two parts, the displacement within the loaded circle of radius a, $(r \leq a)$, and points outside the radius $(r > a)$.

$$w_0 = \begin{cases} \frac{4(1-\nu^2)qa}{\pi E} \int_0^{\pi/2} \sqrt{1 - (r^2/a^2)\sin^2\theta}\, d\theta & \text{for } r \leq a \\ \frac{4(1-\nu^2)qr}{\pi E} \times \left[\int_0^{\frac{\pi}{2}} \sqrt{1 - (a/r)^2 \sin^2\theta}\, d\theta - \left[1 - \frac{a^2}{r^2}\right] \int_0^{\frac{\pi}{2}} \frac{d\theta}{\sqrt{1-(a/r)^2\sin^2\theta}} \right] & \text{for } r > a \end{cases}$$

where,

$$\begin{aligned} \nu &= \text{Poisson's ratio} \\ E &= \text{Young's modulus} \\ a &= \text{radius of the asperity} \\ r &= \text{the distance from the center of the asperity} \\ q &= \frac{f}{\pi a^2} = \text{stress acting on the asperity} \\ f &= \text{force over an asperity} \end{aligned}$$

This displacement can be written in terms of the change in height Δh_i by using,

$$\Delta h_i = \frac{f_i h_i}{\pi a^2 E}. \tag{3.2}$$

To solve this system of linear equations, the conjugate gradient method was chosen [13] because it reduces the problem to a matrix-vector multiplication. The computation time for the solver

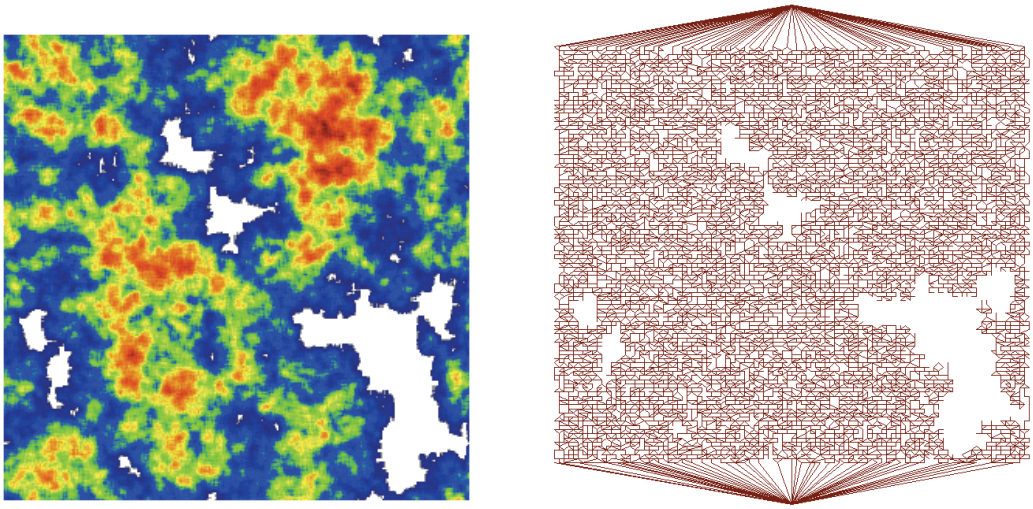

FIG. 2. *(Left) Example fracture geometry, where white is contact area and the range blue-red are increasing apertures. (Right) The resulting pipe network generated using the elliptical pipe network method.*

was reduced by recognizing that long range interactions can be approximated accurately by Taylor expanding the half-space's displacement for large radii. By using this approximation, the matrix-vector product can be rapidly calculated by using the Fast Multipole Method (FMM), [13].

The method described above will compute the fracture deformation with free boundaries. This will effectively simulate the deformation of a fracture in a laboratory setting. In the laboratory, the fractured bulk rock is usually less than a meter in size and either cubic or cylindrical in shape. When placed under a constant displacement load, contact points near the edges will have less support than those near the center, leading to a non-uniform closure. This is fundamentally different than what would be found in the field. Field measurements of fracture specific stiffness will probe local parts of larger fractures. To simulate this scenario, periodic boundary conditions were introduced to the linear system of equations (Equation 3.1) by introducing an "external" lattice of multipole moments in the FMM calculation [8, 7].

4. Flow Model. To investigate the relationship between the mechanical and hydraulic properties of fractures, a flow model is also required. The hydraulic properties of the simulated fractures considered in this study were calculated numerically using a network model similar to that of Yang et al. [19, 20], Tran [17], and Cheng et al. [3]. In this model, the aperture distribution is replaced by a connected graph starting from one inlet node and ending with one outlet node (see Figure 2).

This differs from other models in that it is not direction blind, i.e. global flow and local flow are assumed to be in the same direction. Each row of aperture elements perpendicular to the flow is considered in turn and the large regions of non-zero apertures are brought together into a single large elliptical pipe (Figure 3). Between the rows, flow is calculated based on the analytic solution to flow in an elliptical pipe with a hydraulic resistance based on the apertures,

$$R = \frac{4f\mu\Delta l\sqrt{K}(K+1)}{\pi a^4} \qquad \text{with,}$$
$$f = \frac{\pi a_1 b_1 + \pi a_2 b_2}{2A_{avg}} \qquad \text{and}$$
$$K = (a/h)^2 .$$

Above, a_i and b_i $i = 1, 2$, are the major and minor axes of the two ellipses between rows, a is the average minor axis between the rows, h is half the maximum aperture of the larger ellipse, Δl is

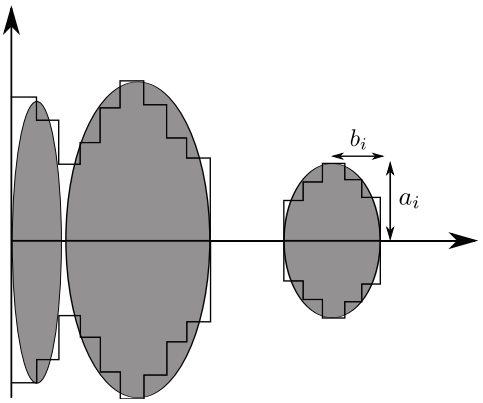

FIG. 3. *Side view of multiple apertures being converted to larger elliptical cross sections. This represents a row of a fracture geometry, perpendicular to the flow direction.*

the distance between the center of the two elements, and finally A_{avg} is the average area of the two ellipses.

This model is preferred over the bi-lattice grid method, used in [13], because it is computationally more efficient (run times are 4-10 times faster) and it was shown to model 2D micro-model experimental data more accurately [3].

5. Results and Discussion.

5.1. Finite-size Scaling due to Fracture generation. This study begins by first investigating the scaling properties due to the generation of synthetic fractures without the influence of mechanical deformation. Fractures were generated at the five scales listed in Table 2.1 and the range of NPTS was chosen such that the void area fraction varied from approximately 30% to 80%. Firstly, the probability of a spanning cluster is shown in Figure 4. As expected, the sharp threshold at large scales "smears" out as the scale decreases. The data is well approximated by an incomplete Beta function and was used in the fit shown. When applying renormalization group theory, we were attempting to find a point in which the renormalization, $\mathcal{R}$, does not change the value of interest. So, if x is a measured property of the system,

$$\mathcal{R}[x] = x. \tag{5.1}$$

When this is done, the fixed point at a given scale has been found. Applying this to the problem at hand, the intersection between the fitted lines and the line $y = x$ were found. Essentially, the right hand side of Equation 5.1 was moved to the left hand side and the equation was solved for x at each scale. These scale dependent fixed points were then extrapolated to find the threshold at the infinite limit. It was found that the critical area fraction, A_c, was approximately 0.608. Secondly, flow calculations were conducted on the generated fractures with constant aperture. The results are shown in the right hand plot of Figure 4. It is clearly seen that there are two regions of interest. For high area fractions, the scale effect cannot be seen and is viewed as an *Effective Medium*. As the area fraction, A_f, approaches the critical threshold, the flow rates enter the region labeled *Critical Region*, where the scale of the system dominates the flow rate. This behaves much like the spanning probability in that, as the scale decreases, the flow rate cutoff also smears out over the threshold. The flow rate, q, can be written in a finite-size scaling form as follows,

$$q(A_f - A_c; L) = L^{-t/\nu}\mathcal{F}\left((A_f - A_c)L^{1/\nu}\right). \tag{5.2}$$

Where $\nu = 4/3$, not to be confused with the Poisson ratio, is the correlation exponent in 2D Percolation Theory and t is the flow exponent that must be found. The function $\mathcal{F}$ is called a

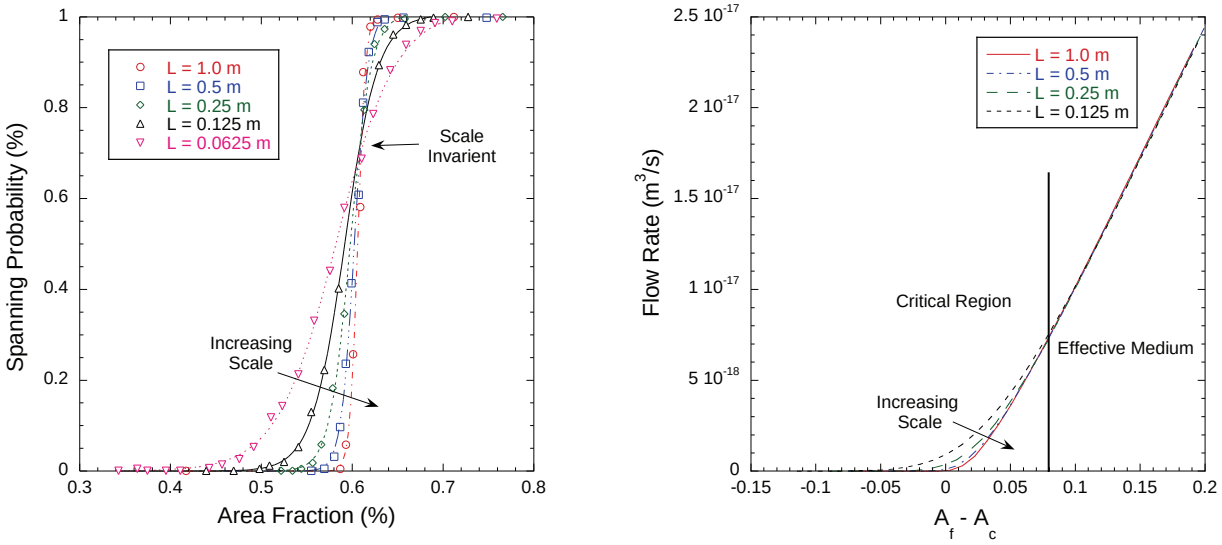

FIG. 4. *(Left) Finite-size scaling of percolation threshold solely due to geometry. (Right) Fluid flow critical scaling near threshold, $A_c \approx 0.6$, and the flow critical exponent is extracted.*

universal function that holds the underlying physics of fluid flow. The elliptical pipe network, described above, was used to obtained F computationally. Written in this form, the flow reduced to a simple power law with respect to the scale of the system when at threshold, $A_f = A_c$. By extrapolating the flow rate at the infinite threshold, it was shown that the flow has the expected power law dependance with respect to scale. The critical exponent for fluid flow was found by fitting a power law to this extrapolation and was found to have an exponent of $t/\nu = 0.963$. While this case study is only for constant aperture fractures, it was used to test the finite-size methodology on our flow codes. While flow exponents are not universal, this example is analogous to the 2D random resistor network found in Stauffer [15], who found $t/\nu = 0.975$, which gives confidence to our implementations.

5.2. Mechanical Finite-size Scaling. After understanding the threshold associated with fluid flow, due to fracture generation, scaling of the mechanical properties was investigated. Conceptually, this was much more simple. In the case of fluid flow, the threshold occurs when the fracture no longer supports flow. The analogous property for fracture stiffness is the force transmitted through the fracture plane (into the page). The threshold is immediately realized as the point when there is no contact between the two rough surfaces. At this point, no force can be transmitted through the fracture, thereby setting the fracture specific stiffness to zero. As soon as points come into contact, the fracture begins to resist deformation leading to a non-zero stiffness. The question that arises concerns the criticality of this fixed point. Like with fluid flow, the fracture specific stiffness is plotted as a function of the contact area fraction, shown in Figure 5. It is quickly observed that there is in fact no critical scaling for both laboratory and field-type fractures. All of the scales lie on the same curve. Again, deformation calculations for field-type fractures use periodic boundary conditions and laboratory-type fractures use free boundary conditions.

The last item that was considered before analyzing the full hydromechanical scaling is understanding how the deformation affects the flow threshold. Before, the critical threshold was only considered during the generation of a fracture; however, this was not the whole story. When a rock is fractured, it has a maximum flow rate when no load is applied. As the normal load increases, two changes occur: (1) apertures begin to shrink, and (2) apertures change to welded contact area (as far as flow is concerned). This may seem quite similar to the generation setting in section 5.1,

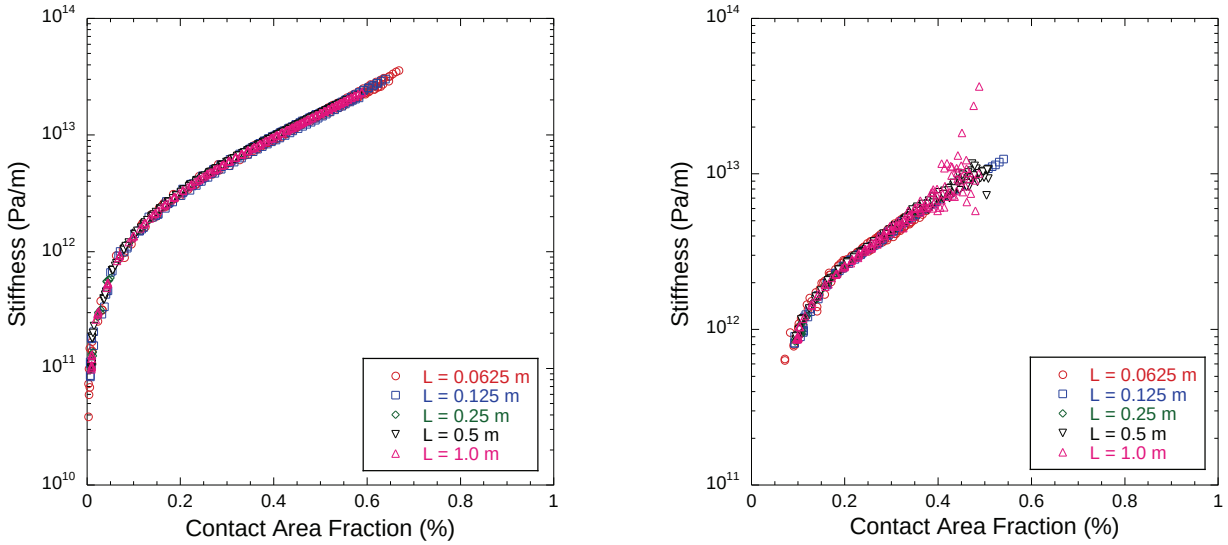

FIG. 5. *Stiffness plotted as a function of contact area fraction for both laboratory (left) and field (right) scales.*

but now a major difference between field and laboratory-type fractures becomes apparent. Field-type fractures have support from both contact area inside and outside the area of interest, while laboratory-type ones will only have support from inside. Because of this, the contact area will grow uniformly across the fracture plane for field scale fractures. For the laboratory scales, the contact area will grow from the edge of the fracture toward the center.

In this case study, fractures were generated using the parameters found in Table 2.1. The deformation calculation was very expensive, so measuring the spanning probability over a given range of area fractions directly was not feasible. Instead, the *probability distribution function* for the threshold was estimated as was done by Reynolds *et al.* [14] for square lattice large-cell renormalization. Specifically, the normal load applied was increased until the spanning cluster no longer extended across the fracture. The load was then brought backward (or forward) half a step 10 times, halving each step, depending on whether the fracture percolated or not. This allowed the solver to approximate the exact load of the threshold up to less than 0.1 % contact area. The spanning probability was the *cumulative distribution function* of this random variable and was analyzed in Figure 6. The right hand side plot shows a clear scaling behavior similar to what was found earlier, as shown in Figure 4, with a clear scale invariant fixed point. The infinite threshold value was extracted as it was before and found to be $A_c \approx 0.568$. The left hand side of Figure 6 shows the spanning probability of laboratory-type fractures. Each scale still has a "smeared" threshold, but there is no clear scale invariant threshold. The threshold appears to shift with scale. It fails because one of the main assumptions in scaling theory is that, when dealing with a system of scale L, the moments of any subsample of scale $L' = L/b$ are independent of the location from which the subsamples were taken. Yet in this case, samples taken from the edges will have higher contact areas from those in the center. Therefore, the threshold is dominated by edge effects.

5.3. Hydromechanical Scaling. Now that the threshold behavior of both the mechanical and hydraulic properties are understood independently, the next step is to investigate the scaling of the coupled system. Since laboratory samples do not have a well defined scaling threshold, only field-type fractures were considered. One hundred samples were generated, using the parameters in Table 2.1, and stressed to a load of 75 MPa in approximately 80 steps. The permeability was then computed at each step in stress. Now, the apertures were *not* constant and the moments of the fracture geometry depend on deformation rather then generation. Therefore, the flow exponent

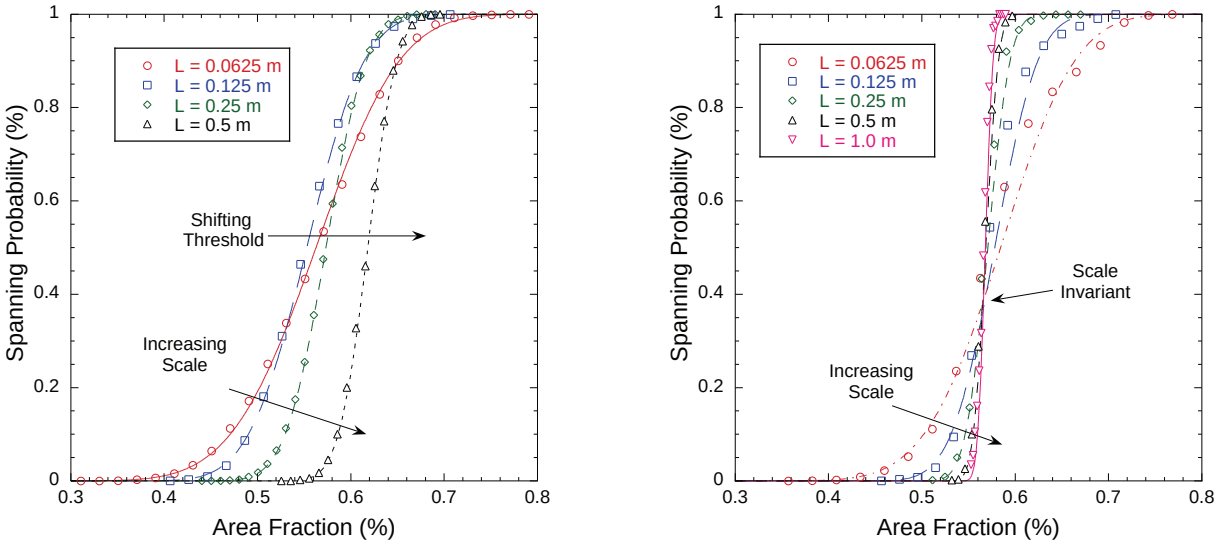

FIG. 6. *Finite-size scaling of percolation threshold solely due to deformation of laboratory (left) and field (right) type fractures.*

must be recomputed. The fluid flow finite-size scaling relationship (Equation 5.2) became,

$$q(A_f(\sigma) - A_c; L) = L^{-t/\nu}\mathcal{F}\left((A_f(\sigma) - A_c)L^{1/\nu}\right), \tag{5.3}$$

where the only difference is that now the area fraction is a function of stress, σ. So now, each graph will be plotted parametrically in stress. Plots of the average flow value as a function of area fraction are shown on the left figure of Figure 7. The vertical dotted line shows the infinite threshold. Flow values were pulled near threshold and plotted against their respective scales (small plot in Figure 7) to extract the exponent. A power law fit calculated that the exponent t/ν is 2.384. Like in section 5.1, there is a clear Effective Medium and Critical regime. The scaled permeability is shown on the right figure of Figure 7. It displays the expected data collapse at threshold.

Lastly, the permeability was plotted against the fracture specific stiffness in Figure 8 with stress as a parametric variable. As the data indicates, there is an Effective Medium regime for low stiffnesses (high area fractions). However, as the load increases the scale dependence appears. This is expected since flow becomes critical. This spread is removed in the critical regime by scaling the permeability by $L^{t/\nu}$, as shown in the right hand side of Figure 8. The fixed point is then scale invariant while the scale dependance is transferred to the Effective Medium regime.

6. Conclusions. Researchers have long sought the ability to predict permeability of rock fractures in the subsurface. Difficulties arise in this prediction since the subsurface is made up of processes that occur on many length and temporal scales. Renormalization group theory provides a powerful framework to incorporate the scale of a system into its underlying statistical properties, which in our case would be the hydrodynamic properties.

In this paper, the computational methods required to study the hydromechanics of single fractures were described. The problem was then separated into three parts: (1) a standard 2D percolation theory description of fluid flow using the stratified percolation method for uncorrelated constant aperture fractures; (2) the difference in threshold behavior between laboratory and field-type fractures and their criticality; and lastly (3) the full hydromechanical scaling.

When describing the unit aperture flow near threshold, it was found that the critical exponent is $t/\nu = 0.963$. Next, the authors showed that the fracture specific stiffness does not contain any critical scaling. However, the difference between laboratory and field-type fractures became

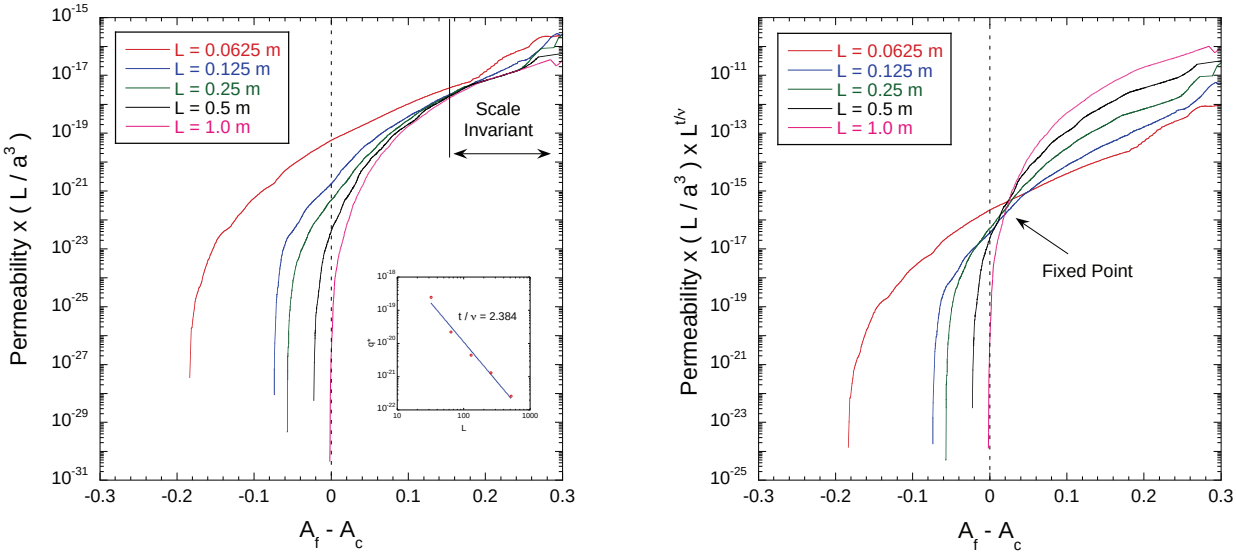

FIG. 7. *Plots illustrating the finite-size scale effect of permeability due to deformation. The left side shows the raw data while the right plot removed the scatter near threshold, $A_f = A_c$, by scaling the permeability by $L^{t/\nu}$. The inner plot on the left side shows the extraction of the exponent t/ν.*

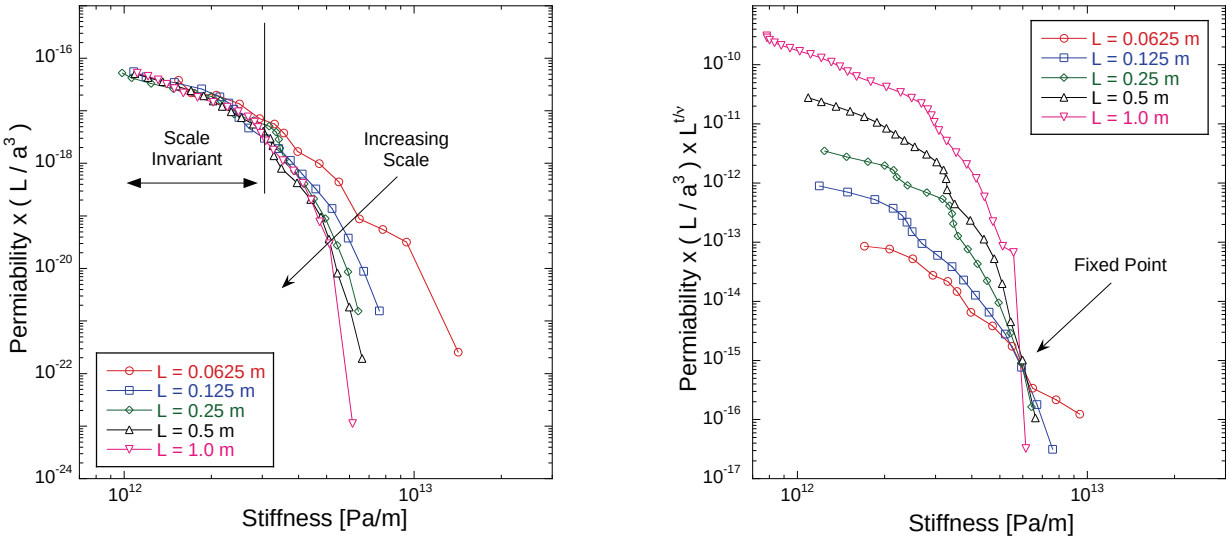

FIG. 8. *(Left) Permeability plotted against fracture specific stiffness with stress as a parametric parameter. (Right) The same data as the left while scaling the perimability by $L^{t/\nu}$.*

quite clear. Field-type fractures displayed a clear scaling near threshold and were extrapolated to the infinite limit, while laboratory-type fractures featured a shifting threshold. Lastly, the critical exponents pertaining to permeability were extracted when the fractures were subject to normal loads. It was found that the critical flow exponent is $t/\nu = 2.384$. This was then used to collapse the permeability-stiffness curves so that they became scale invariant at threshold.

7. Acknowledgments. The authors wish to acknowledge Joe Morris for his assistance with code development. The authors wish to acknowledge support of this work by the Geosciences Research Program, Office of Basic Energy Sciences US Department of Energy (DEFG02-97ER14785

08), the GeoMathematical Imaging Group at Purdue University and from the Computer Research Institute At Purdue University.

REFERENCES

[1] FM Borodich and DA Onishchenko. Similarity and fractality in the modelling of roughness by a multilevel profile with hierarchical structure. *International Journal of Solids and Structures*, 36(17):2585–2612, 1999.
[2] SR Brown and CH Scholz. Closure of random elastic surfaces in contact. *Journal Of Geophysical Research-Solid Earth And Planets*, 90(NB7):5531–5545, 1985.
[3] J.T. Cheng, J.P. Morris, J. Tran, A. Lumsbaine, N.J. Giordano, D.D. Nolte, and L.J. Pyrak-Nolte. Single-phase flow in a rock fracture: micro-model experiments and network flow simulation. *International Journal of Rock Mechanics and Mining Sciences*, 41:687–693, 2004.
[4] PWJ Glover, K Matsuki, and K Hayashi. Synthetic rough fractures in rock. *Journal of Geophysics Research - Solid Earth*, 103:9609–9620, 1998.
[5] J. A. Greenwood and J. B. P. Williamson. Contact of nominally flat surfaces. *Proceedings of the Royal Society of London. Series A, Mathematical and Physical Sciences*, 295(1442):300–319, 1966.
[6] D.L. Hopkins. *The Effect of Surface Roughness on Joint Stiffness, Aperture, and Acustic Wave Propagation*. PhD thesis, 1990.
[7] J. Kurzak and B. M. Pettitt. Fast multipole methods for particle dynamics. *Molecular Simulation*, 32(10-11):775–790, 2006.
[8] C. G. Lambert. Multipole-based algorithms for efficient calculation of forces and potentials in macroscopic periodic assemblies of particles. Technical report, Duke University, 1994.
[9] DD Nolte and LJ Pyrak-Nolte. Stratified continuum percolation - scaling geoemetry of hierarchical cascades. *Physical Review A*, 44(10):6320–6333, 1991.
[10] DD Nolte and LJ Pyrak-Nolte. Coexisting two-phase flow in correlated two-dimensional percolation. *Physical Review E*, 56(5, Part A):5009–5012, 1997.
[11] DD Nolte, LJ Pyrak-Nolte, and NGW Cook. The fractal geometry of flow paths in natural fractures in rock and the approach to percolation. *Pure and Applied Geophysics*, 131(1-2):111–138, 1989.
[12] H. Peitgen and D. Saupe. *The science of fractal images*. Springer, 1988.
[13] L.J. Pyrak-Nolte and J.P. Morris. Single fractures under normal stress: The relation between fracture stiffness and fluid flow. *International Journal of Rock Mechanics and Mining Sciences*, 37:245–262, 2000.
[14] Peter J. Reynolds, H. Eugene Stanley, and W. Klein. Large-cell monte carlo renormalization group for percolation. *Phys. Rev. B*, 21:1223–1245, Feb 1980.
[15] Dietrich Stauffer and Amnon Aharony. *Introduction to Percolation Theory*. CRC Press, 1985.
[16] S.P. Timoshenko and J.N. Goodier. *Theory of elasticity 3rd ed.* McGraw-Hill, 1970.
[17] J.J. Tran. *Efficient simulation of multiphase flow in three-dimensional fracture netowrks*. PhD thesis, 1998.
[18] R. Walsh, C. McDermott, and O. Kolditz. Numerical modeling of stress-permeability coupling in rough fractures. *Hydrogeology Journal*, 16:613–627, 2008.
[19] G. Yang, N.G.W. Cook, and L.R. Myer. Network modelling of flow in natural fractures as a guide for efficient utilization of natural resources. *Proceedings of 30th US Symposium on Rock Mechanics*, pages 57–64, 1989.
[20] G. Yang, L.R. Myer, S.R. Brown, and N.G.W. Cook. Microscopic analysis of macroscopic transport-properties of single natural fractures using graph-theory algorithms. *Geophys Res Lett*, 1995.